

# Accuracy analysis of a Hartmann-Shack wavefront sensor operated with a faint object

Genrui Cao

Xin Yu

Beijing Institute of Technology  
Department of Optical Engineering  
Beijing 100081, China

**Abstract.** A detailed analysis of the characteristics, regularities, and relationships of the centroiding errors of image spots caused by discrete and limited sampling, photon noise, and readout noise of the detector in a Hartmann-Shack wavefront sensor, wherein an image intensified charge-coupled device used as a photon detector is presented. The theoretical analysis and experimental results herein prove useful for optimum design and application of the sensor.

*Subject terms:* adaptive optics; wavefront sensor; statistics.

*Optical Engineering* 33(7), 2331–2335 (July 1994).

## 1 Introduction

As a servo loop error sensor, the wavefront sensor is one of the key parts in the adaptive optical system. Numerous as the types of wavefront sensor may be, the choice is critically restricted by the limited signal photons and limited detect time for astronomical applications. It is preferable to use the Hartmann-Shack (H-S) wavefront sensor using an intensified charge-coupled device (ICCD) as a photon detector because they are highly sensitive, flexible, and complex. We first discuss in detail the characteristics, regularities, and relationships of centroiding errors of image spots, caused by limited and discrete sampling, photon noise, and readout noise. Then we introduce an experimental device of the H-S wavefront sensor. Finally, we provide an experimental and theoretical estimation of its performance.

## 2 Analyses of Centroiding Accuracy

A schematic configuration of the H-S wavefront sensor is shown in Fig. 1. As is well known, the radical limitation of the H-S type wavefront sensor is that of centroiding image spot accuracy. Centroiding errors, as a matter of fact, come mainly from the incident photon noise, the discrete and limited sampling of the image intensity distribution, and the readout noise of the detector unit. Goad et al.,<sup>1</sup> Kane et al.,<sup>2</sup> and Morgan et al.<sup>3</sup> indicated the degradation factor of centroiding accuracy connected with the pixel dimensions, quantity, and duty ratio of pixels. Morgan et al. derived an approximate equation from the estimation of image spot centroiding error in the presence of readout noise with the assumption of uniform image intensity distribution on the pixels. Here, we provide a detailed theoretical and experimental analysis based on our own work.

### 2.1 Sampling Error

The centroid position of an image spot with profile  $I(X)$  is defined as (for the 1-D case, which is similar to the 2-D case)

$$X_{ct} = \frac{\int I(X)X \, dX}{\int I(X) \, dX} \quad (1)$$

For an ideal photodetector array of finite size, quantity, and duty ratio of pixels, the detected centroid position of image spot would be

$$X_{cd} = \frac{\sum_{i,j}^{L,M} X_i P_{i,j}}{\sum_{i,j}^{L,M} P_{i,j}}, \quad (2)$$

where

$$P_{i,j} = D(X)W(X) \int_{\gamma_j - b/2}^{\gamma_j + b/2} dY \int_{X_i - a/2}^{X_i + a/2} dX$$

is the detected photon events in the  $(i,j)$ 'th pixel;

$$D(X) = \sum_{i=-L/2}^{L/2} \prod [(X - 0.5 - i)/\gamma_X]$$

is the structure function of detector array;  $W(X) = \prod(X/L)$  is the subwindow function divided for the subaperture on a detector array;  $\gamma_X$  is the duty ratio of pixels in the  $X$  direction;  $a$  and  $b$  are the sizes of pixels in the  $X$  and  $Y$  directions, respectively; and  $L$  and  $M$  are the numbers of pixels in the  $X$  and  $Y$  directions, respectively, within the same subwindow.

Figure 2 shows the geometrical significance of  $D(X)$  and  $W(X)$ . Figure 3 indicates the sampling errors of the centroiding for different image spot widths. It can be seen from Fig. 3 that

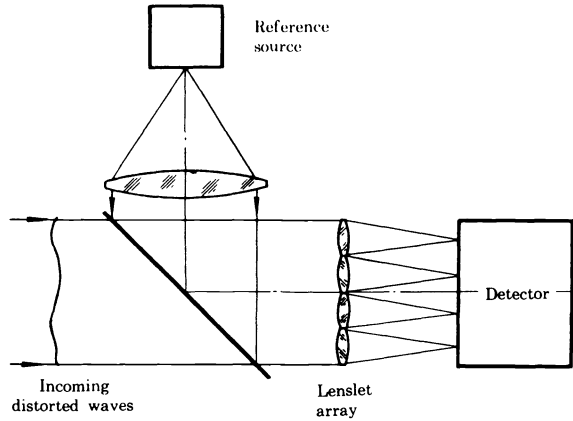


Fig. 1 Schematic configuration of the H-S wavefront sensor.

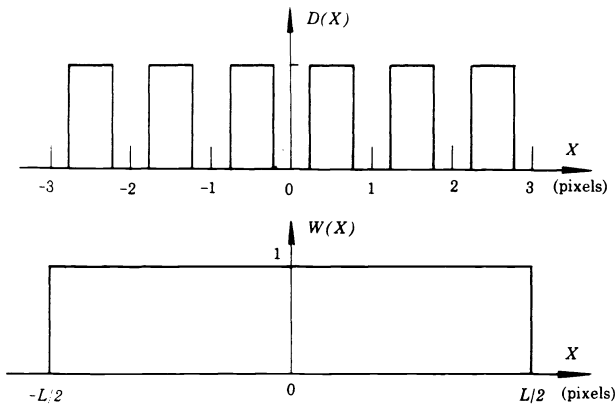


Fig. 2 Geometrical significance of the CCD structure and subwindow functions.

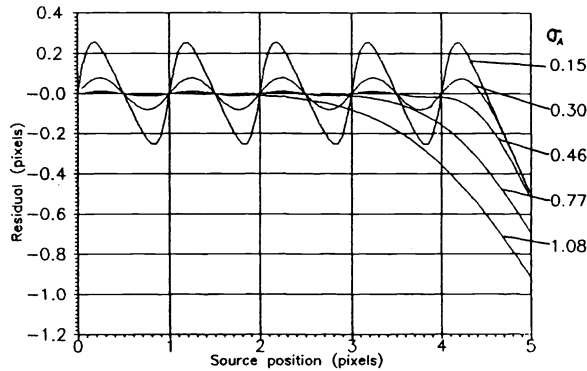


Fig. 3 Sampling error of the centroiding for different image spot widths.

as the Gaussian width  $\sigma_A$  of an image spot increases, the magnitude of the discrete sampling errors will decrease sharply. But it will be restricted by the cutoff errors at the window edge and the readout noise, discussed later. Calculations made have also shown that if the duty ratio of pixels goes down, the discrete sampling errors will go up. However, they are almost independent of the subwindow size. If the ratio of the image spot width to the pixel size  $\sigma_A/a$  is larger than about 0.5, the root mean square of centroiding error

$\sigma_{X_{cs}}$  caused by discrete and limited sampling will be less than  $0.02\sigma_A$ , whose effects can therefore be neglected.

## 2.2 Readout Noise Error

Various and complicated as noise sources in a wavefront sensor may be, they are mainly made up of the so-called readout noise at the output or input sides of the sensor. If only the readout noise of the detector is taken into consideration, the variance of detected centroid positions of an image spot can be derived from Eq. (2) as

$$\sigma_{X_{cr}}^2 = \frac{\sigma_U^2}{V^2} + \frac{U^2 \sigma_V^2}{V^4} - \frac{2U\sigma_{UV}}{V^3}, \quad (3)$$

where  $U = \sum_{i,j}^{L,M} X_i P_{ij}$ ;  $V = \sum_{i,j}^{L,M} P_{ij}$ ;  $\sigma_U^2$  and  $\sigma_V^2$  are the variances of  $U$  and  $V$ , respectively; and  $\sigma_{UV}$  is the covariance of  $U$  and  $V$ . From the calculation, it can be deduced that

$$\begin{aligned} \sigma_U^2 &= \sum_{i,j}^{L,M} X_i^2 S_{ij}^2 + \sum_{i,j \neq kl}^{L,M} S_{ijkl} X_i X_k, \\ \sigma_V^2 &= \sum_{i,j}^{L,M} S_{ij}^2 + \sum_{i,j \neq kl}^{L,M} S_{ijkl}, \\ \sigma_{UV} &= \sum_{i,j}^{L,M} X_i S_{ij}^2 + \sum_{i,j \neq kl}^{L,M} S_{ijkl} X_i, \end{aligned} \quad (4)$$

where  $S_{ij}^2$  is the variance of photon events  $P_{i,j}$  counted at the  $(i,j)$ 'th pixel and  $S_{ijkl}$  is the covariance for the  $(i,j)$ 'th and  $(k,l)$ 'th pixels in a subwindow.

If only the readout noise  $\sigma_r$  is taken into account, and a uniform response of pixels is assumed, we have

$$S_{ij}^2 = \sigma_r^2. \quad (5)$$

Because the number of pixels assigned for each subwindow is usually big enough, we are justified to set  $S_{ijkl} = 0$ . Substituting Eqs. (4) and (5) into Eq. (3), we find

$$\begin{aligned} \sigma_{X_{cr}}^2 &= \frac{\sigma_r^2}{V^2} \left( \sum_{i,j}^{L,M} X_i^2 + LM X_c^2 - 2X_c \sum_{i,j}^{L,M} X_i \right) \\ &= \frac{\sigma_r^2}{V^2} M \left( \sum_i^L X_i + L X_c^2 \right) \\ &= \frac{\sigma_r^2}{V^2} ML \left( \frac{L^2 - 1}{12} + X_c^2 \right), \end{aligned} \quad (6)$$

where  $X_c$  is the average centroid position of image spot in the subwindow as the image spot is wobbled by the air turbulence.

Because the average centroid position of image spot in each subwindow can be shifted to be coincident with its origin of coordinates by adjustment, the variance of image spot centroid position  $\langle X_c^2 \rangle$  can be related to the variance of incident wavefront tilt  $\langle \alpha^2 \rangle$  within subaperture. In the case of subaperture diameter being equal to the atmospheric coherence length  $r_0$ , the variance of incident wavefront tilt by definition<sup>4</sup> should be

$$\langle \alpha^2 \rangle = 6.88 / (K^2 r_0^2) , \quad (7)$$

where  $K = 2\pi/\lambda$ . From geometrical optics, we can relate  $X_c$  and  $\alpha$  as

$$X_c = \alpha \frac{r_0}{d} f \\ = 0.417\lambda F^\# , \quad (8)$$

where  $F^\#$  is the  $f/\#$  of lenslet and  $r_0/d$  refers to the angle magnification at the entrance pupil of lenslet.

Generally, the intensity distribution of a diffracted image spot can be denoted by the Gaussian distribution matched at the  $e^{-1}$  points. The rms width of an image spot diffracted by the circular aperture (CA) or the square aperture (SA) are, respectively,

$$\sigma_A = 0.431\lambda F^\# \quad (\text{for CA}) , \quad (9)$$

$$\text{or } \sigma_B = 0.358\lambda F^\# \quad (\text{for SA}) . \quad (10)$$

Comparing the Eqs. (9) and (10) with Eq. (8), we can deduce

$$\langle X_c^2 \rangle = 0.936\sigma_A^2 \quad (\text{for CA}) , \quad (11)$$

$$\text{or } \langle X_c^2 \rangle = 1.36\sigma_B^2 \quad (\text{for SA}) . \quad (12)$$

Therefore, Eq. (6) can be rewritten as

$$\sigma_{X_{cr}}^2 = \frac{\sigma_r^2}{V^2} ML \left( \frac{L^2 - 1}{12} + 0.936\sigma_A^2 \right) \quad (\text{for CA}) , \quad (13)$$

$$\text{or } \sigma_{X_{cr}}^2 = \frac{\sigma_r^2}{V^2} ML \left( \frac{L^2 - 1}{12} + 1.36\sigma_B^2 \right) \quad (\text{for SA}) . \quad (14)$$

It can be found that the centroiding errors of image spots are dependent not only on the readout noise itself but also on the size of the subwindow assigned for each image spot on the ICCD and the total number of photons included in each subaperture. Reducing the size of the subwindow can help to reduce effectively the centroiding errors caused by the readout noise, as shown in the experimental results of Table 1. However, it will be also restricted by the sampling errors and dynamic range of image spot wobbling. Therefore, a trade-off should be made between the readout noise and the subwindow size, pixel size, and image spot size.

As to the influence of photon noise on the centroiding error or image spot, substituting  $\sigma_r^2$  in Eq. (5) with  $P_{i,j}$ , we find the well-known equation,

$$\sigma_{X_{cp}}^2 = \sigma_A^2 / V . \quad (15)$$

### 2.3 Performance Estimation

Because all of the previously mentioned errors are independent of each other, the complete centroiding errors of image

spot can be summarized as

$$\sigma_{X_c}^2 = \sigma_{X_{cs}}^2 + \sigma_{X_{cp}}^2 + \sigma_{X_{cr}}^2 . \quad (16)$$

Within a subaperture, the maximum optical path difference (OPD) error concerned with the centroiding error of image spot is

$$W_{\max} = \sqrt{2}\sigma_{X_c} / F^\# , \quad (17)$$

and the rms of OPD error is

$$\Delta W_{\text{rms}} = \sqrt{2}\sigma_{X_c} / (4F^\#) \\ = 0.152\lambda\sigma_{X_c} / \sigma_A \quad (\text{for CA}) , \quad (18)$$

$$\text{or } \Delta W_{\text{rms}} = \sqrt{2}\sigma_{X_c} / (\sqrt{12}F^\#) \\ = 0.146\lambda\sigma_{X_c} / \sigma_B \quad (\text{for SA}) . \quad (19)$$

Note that in the case of square subaperture,  $F^\#$  is understood as the ratio of focal length of the lenslet to its clear aperture size of square. For example, if we have  $\sigma_B = 0.5$ ,  $L = M = 12$ ,  $\sigma_r = 0.1$ ,  $V = 100$ , and  $a = b$ , then the variance of centroiding errors calculated from the preceding related equations can be deduced as

$$\sigma_{X_c}^2 = \sigma_{X_{cs}}^2 + \sigma_{X_{cp}}^2 + \sigma_{X_{cr}}^2 = 0 + 0.0025 + 0.0018 = 0.0043$$

$$\text{and } W_{\text{rms}} = 0.146\lambda\sigma_{X_c} / \sigma_B = \lambda/52 \quad (\text{for SA}) ,$$

where the units of  $\sigma_B$ ,  $L$ ,  $M$ , and  $\sigma_{X_c}$  are the pixel size, whereas the units of  $\sigma_r$  and  $V$  are the photon event.

### 3 Experimental Results

Figure 4 shows an experimental H-S wavefront sensor device using an ICCD as a photon detector in which the lens array consists of 76 lenslets with the 255-mm focal length and a clear aperture of  $1.5 \times 1.5 \text{ mm}^2$ . The image spot array is thus enhanced by an image intensifier coupled to a high-frame-rate CCD with a most powerful relay lens. An associated photon counter is used for calibrating magnitude of the light source.<sup>5</sup> An optical wedge is used for simulation of the wave-

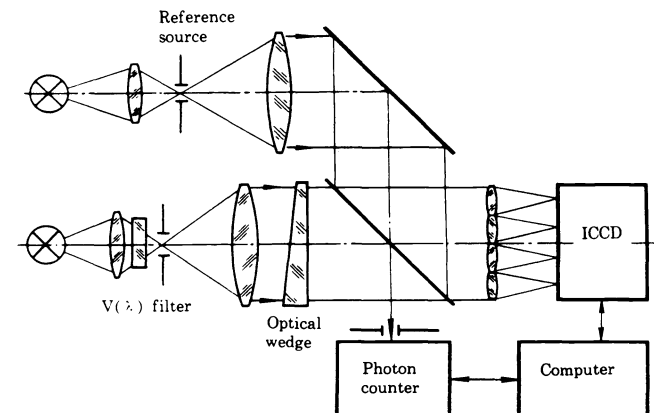


Fig. 4 Experimental H-S wavefront sensor device.

**Table 1** Experimental results for centroiding errors and the corresponding subwindow sizes.

$M \times L (\text{pixels})$	$13 \times 13$	$21 \times 21$	$33 \times 33$	$41 \times 41$
$\sigma_{X_c} (\text{pixels})$	$0.46 \times 10^{-3}$	$0.98 \times 10^{-3}$	$1.9 \times 10^{-3}$	$44 \times 10^{-3}$

front tilt. The  $V(\lambda)$  filter in the system can be used to eliminate the spectral response difference between the photon counter and the ICCD.

For an actual ICCD detector, the major source of the centroiding errors comes from the readout noise and the photon noise. Therefore it is meaningful to measure the readout noise of the detector unit directly. Generally speaking, the noise made in an ICCD detector operated in multiphoton mode consists mainly of the inherent photon noise of the photon signals and the readout noise of detector and its associated circuits. Because they are independent of each other, the variance of the total noise can be measured at the output end of ICCD as<sup>6,7</sup>

$$\sigma_0^2 = g^2 \sigma_p^2 + g^2 \sigma_r^2, \quad (20)$$

where  $g$  is the photon gain of ICCD detector and  $\sigma_p^2$  is the variance of photon events, which is equal to its mean value  $p_i$  according to the Poisson distribution. Hence, we have

$$\begin{aligned} \sigma_0^2 &= g^2 p_i + g^2 \sigma_r^2 \\ &= g p_0 + g^2 \sigma_r^2, \end{aligned} \quad (21)$$

where  $p_0$  is the mean number of photons at the output side of the ICCD. For computer data processing convenience, this equation can be modified as

$$k^2 \sigma_0^2 = k^2 g p_0 + k^2 g^2 \sigma_r^2, \quad (22)$$

where  $k$  is the convertor factor of single photon event into digits in the calculations. If we let  $k \sigma_0 = n_0$ ,  $kg = G$ , and  $k p_0 = P_0$ , then we have

$$n_0^2 = G P_0 + G^2 \sigma_r^2. \quad (23)$$

It is evident that by recording two frames of flat-field  $P_0$  and  $P'_0$  and one frame of dark-field  $D$  for different photon signal levels, we can deduce a series of data about total noise variances and their corresponding mean signals calculated from the following equations, respectively,

$$n_0^2 = \frac{1}{2LM} \sum_{i,j}^{L,M} (P_{0ij} - P'_{0ij}) \quad (24)$$

$$\text{and } P_0 = \frac{1}{2LM} \sum_{i,j}^{L,M} [(P_{0ij} - D_{ij}) + (P'_{0ij} - D_{ij})]. \quad (25)$$

Figure 5 shows the experimental results of the readout noise  $\sigma_r$  and the digitalized photon gain  $G$  of an ICCD detector, where the readout noise is quite significant, because the ICCD was not being cooled. The experiments also show that an accuracy of  $\lambda/14$  rms OPD has been achieved corresponding to a  $100 \times 100$  mm<sup>2</sup> subaperture and 1 ms of sampling time for a sixth visible magnitude of object.

#### 4 Conclusions

The ICCD detector has displayed a good performance with an H-S wavefront sensor operated with the faint objects, but its readout noise, in addition to the photon noise, may seriously degrade the centroiding accuracy of image spot. The

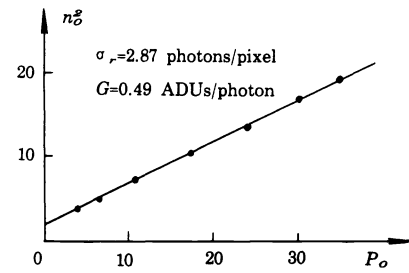


**Fig. 5** Experimental results of the readout noise  $\sigma_r$  and the gain  $G$  of an ICCD detector. (ADU—the minimum unit of digital readout from A/D converter.)

readout noise comes mainly from the image intensifier and can be significantly reduced by cooling its photocathode.

The influence of readout noise on the centroiding errors for the H-S wavefront sensor can be reduced to a considerable degree by appropriately limiting the size of the window assigned for each subaperture on the ICCD and shifting the centers of wobbling image spots to be coincident with their origins of coordinates in each subwindow.

#### Acknowledgments

This work was supported by the Hightech Project of China. We would like to thank Prof. Dazun Zhao for helpful discussion and Mr. Guihua Cui for partial work on computer programming of sampling error.

#### References

1. L. Goad, F. Roddier, J. Beckers, and P. Eisenhardt, "Criteria for the wavefront sensor selection," The NNTT Technology Development Program Report No. 9 (March 1986).
2. T. Y. Kane, B. M. Welsh, C. S. Gardner, and L. A. Thompson, "Wavefront detector optimization for laser guided adaptive telescope," *Proc. SPIE* **1114**, 160–171 (1990).
3. J. S. Morgan, D. C. Slater, J. G. Timothy, and E. B. Jenkins, "Centroid position measurements and subpixel sensitivity variations with the MAMA detector," *Appl. Opt.* **28**(6), 1178–1192 (1989).
4. V. Tatarski, *Wave Propagation in a Turbulent Medium*, McGraw-Hill, New York (1961).
5. G. Cao, X. Yu, R. Gu, R. Zhou, and D. Zhao, "An experimental study on photon noise limited wave front sensor," *Proc. SPIE* **1230**, 456–460 (1990).
6. B. Ye, Xinming, and C. Wang, "The characteristics of CCDs and their evaluation," Publications of Purple Mountain Observatory, **2**(4), 81–92 (1983) (in Chinese).
7. S. Marcus, R. Nelson, and R. Lynds, "Preliminary evaluation of a fairchild CCD-211 a new camera system," *Proc. SPIE* **172**, 207–231 (1979).



**Genrui Cao** graduated from the Department of Optical Engineering, Beijing Institute of Technology, China, in 1963, where he has been a faculty member for about 30 years. Prof. Cao's areas of research are optical testing, image assessment, interferometry, optical fabrication, adaptive optics, and wavefront sensing. He has developed a series of instruments and has published a series of papers and books in these fields. From 1985 to 1987 he worked as a visiting scholar in the fields of large optics testing and scattering at the Optical Sciences Center, University of Arizona.



**Xin Yu** is a professor in and director of the Department of Optical Engineering, Beijing Institute of Technology, China. His research includes infrared technology, gas laser devices, and optoelectronic metrology methods. He currently heads a project in the adaptive optics system with wavefront distortion through atmospheric turbulence, low-light-level wavefront sensors, signal processing, and wide-field and partial correction adaptive optics theory. Prof.

Yu graduated from Beijing Institute of Technology in 1963 and studied as a visiting scholar at State University of New York at Stony Brook from 1984 to 1986.